Available online at www.sciencedirect.com

ScienceDirect

Ceramics International 40 (2014) 729–737

CERAMICS INTERNATIONAL

www.elsevier.com/locate/ceramint

# *In-vitro* characterization of antibacterial bioactive glass containing ceria

Yi-Fan Goh[a], Ammar Z. Alshemary[a], Muhammad Akram[a], Mohammed Rafiq Abdul Kadir[b], Rafaqat Hussain[c,*]

[a]*Department of Chemistry, Faculty of Science, Universiti Teknologi Malaysia, 81310 UTM skudai, Johor Darul Ta'zim, Malaysia*
[b]*Medical Implant Technology Group, Faculty of Biomedical Engineering and Health Science, Universiti Teknologi Malaysia, 81310 UTM Johor Bahru, Malaysia*
[c]*IbnuSina Institute for Fundamental Science Studies, Universiti Teknologi Malaysia, 81310 UTM Johor Bahru, Johor Darul Ta'zim, Malaysia*

Received 22 May 2013; received in revised form 17 June 2013; accepted 17 June 2013
Available online 2 July 2013

**Abstract**

Several compositions of bioactive glass (BG) containing ceria were synthesized from chloride precursor using quick alkali sol–gel method. XRD data revealed the presence of ceria in 5 and 10 mol% Ce samples. SEM and EDX characterization confirmed the nano-size and elemental composition of all samples, while FTIR data indicated that high Ce content has disrupted the silicate network of BG. UV absorption spectrum showed that ceria in BG samples is present in +3 and +4 oxidation states, depending on the initial cerium content. Nitrogen adsorption–desorption isotherm confirmed the mesoporosity of the samples. 5 and 10 mol% Ce samples exhibited significant antibacterial properties compared to 1Ce and 50Si samples. All samples induced the formation of apatite particles with Ca/P ratio close to 1.67 upon immersion in simulated body fluid (SBF), confirming their good bioactivity. For the first time, this study has demonstrated that cerium is a promising candidate to impart BG with excellent antibacterial properties without compromising its bioactivity.


*Keywords:* B. Electron microscopy; Rare earth biomaterials; Sol–gel growth; Nanostructures; Antibacterial properties

## 1. Introduction

Bioactive glass (BG) is a group of biomaterials with a silicate structure of chemical formula $SiO_2$, CaO with or without $P_2O_5$ [1,2]. Since its invention about 40 years ago, it has aroused great interest among material scientists because of its excellent bioactivity that leads to osteointegration [3]. Its bioactivity is characterized by the apatite forming ability on the surface upon immersion in physiological fluid [4]. This has rendered BG its wide use in bone regeneration field, for example periodontal disease [5], coatings of implants [6] and scaffolds [7]. Clinically, bacterial colonization or infections pose a serious threat to the usability of implants and often leads to their failure [8]. Although some BG have been reported to possess antibacterial properties, it is more advantageous to modify BG by incorporating some useful elements into its structure in order to control the release of these ions which are responsible for the antibacterial activity [9].

Cerium, a rare earth element has found numerous industrial applications such as catalysts, fuel additives and colored component doped in glass, however, its potential role in biomedical application has been undervalued. Cerium has been known to exist in different valencies in glass due to its interesting electronic structure, which can be investigated using UV spectroscopy. Cerium has been used in the treatment of severe burns; however, its antimicrobial potential is open to debate since contrasting *in vitro* results are always reported [10]. On the other hand, materials incorporated with Cerium have shown promising antimicrobial activities [11,12], possibly due to its ability to dissociate

*Corresponding author. Tel./fax: +60 7 553 4316
*E-mail address:* rafaqat@kimia.fs.utm.my (R. Hussain).

0272-8842/$ - see front matter © 2013 Elsevier Ltd and Techna Group S.r.l. All rights reserved.
http://dx.doi.org/10.1016/j.ceramint.2013.06.062

outer membrane of bacterial cells from cytoplasmic membrane [13]. Cerium in the form of ceria has been shown to exert toxicity toward bacterial cells through interaction with the cell membrane [14,15]. In previous study of Ce doped BG no $CeO_2$ phases were detected in the XRD even though $CeO_2$ was directly mixed in BG [16]. In another study the preparation of Ce doped BG from cerium (III) nitrate also showed no presence of $CeO_2$ phases, which led them to conclude that the Ce existed as $Ce_2O_3$ in BG [17], however, phase attributed to $Ce_2O_3$ was not detected in their XRD. To best of our knowledge, there is still no report of antibacterial effects of BG containing ceria. Therefore, in this study, *in vitro* bioactivity and antibacterial response towards *Escherichia coli* via quantitative method are studied for BG containing ceria synthesized from chloride precursor.

## 2. Material and methods

### 2.1. Materials

All chemicals used for sol–gel synthesis were reagent-grade, tetraethyl orthosilicate (TEOS, Fluka, Switzerland), calcium nitrate tetrahydrate ($Ca(NO_3)\cdot 4H_2O$, QREC, New Zealand), triethyl phosphate (TEP, Fluka, Switzerland) and cerium chloride heptahydrate ($CeCl_3\cdot 7H_2O$, QREC, New Zealand). 2 M ammonia solution and 2 M nitric acid were prepared by using 37% ammonia solution ($NH_4OH$, QREC, New Zealand) and 65% concentrated nitric acid ($HNO_3$, Fluka, Switzerland). Ethanol ($CH_3CH_2OH$, Fluka, Switzerland) and deionized water were used as solvents in this investigation.

### 2.2. Sol–gel synthesis

Quick alkali mediated sol–gel method [18] was used to synthesize BG containing ceria. TEOS was mixed with 2 M nitric acid to undergo acid hydrolysis for 1 h. This was followed by the addition of TEP, $CaCO_3.4H_2O$, and $CeCl_3\cdot 7H_2O$ with 30 min interval between each addition to allow each reagent to react completely. Finally, the whole mixture was stirred for 1 h to obtain a clear sol. Excess $NH_4OH$ (2 M) solution was added to the resulting solution in an ultrasonic water bath until gelation occurred [19]. The formed gel was dried at 75 °C for 48 h followed by calcinations at 700 °C for 2 h with heating rate 5 °C/min in a muffle furnace. Different compositions of BGs are listed in Table 1

Table 1
Nominal composition of BG.

| Sample code | Composition (mol%) | | | |
|---|---|---|---|---|
| | $SiO_2$ | CaO | $P_2O_5$ | $CeO_2$ |
| 50Si | 50 | 45 | 5 | |
| 1Ce | 50 | 44 | 5 | 1 |
| 5Ce | 50 | 40 | 5 | 5 |
| 10Ce | 50 | 35 | 5 | 10 |

### 2.3. Characterization techniques

#### 2.3.1. X-ray diffraction

Phase composition of synthesized BGs was studied using X-Ray Diffractometer (XRD, Bruker, D8 Advance) at 40 kV and 30 mA utilizing CuKα radiation. The range of $2\theta$ angles was from 20° to 80°, at a step size of 0.02°and step time of 1 s.

#### 2.3.2. UV-NIR spectroscopy

Ultra violet–visible absorption spectra were measured for all samples in the 200–800 nm spectral range, by using the diffuse reflectance technique (UV–vis, Shimadzu, UV-3101PC).

#### 2.3.3. Fourier transform infrared spectroscopy

The infrared spectra of the samples were recorded in a wavenumber range of 450–4000 $cm^{-1}$ using a Fourier Transform Infrared spectrophotometer (FTIR, Jasco, FT/IR-6100).

#### 2.3.4. Low vacuum scanning electron microscope and energy dispersive X-ray spectroscopy

The morphology and composition of calcined BG samples were studied using SEM (SEM, JEOL, JSM-6390) at an operating voltage of 15 kV and Energy Dispersive X-ray Spectrometer (EDX, Hitachi, SwiftED3000) respectively. Before examination, samples were coated with platinum at 20 mA for 40 s. To evaluate particle size distribution, measurements of particles size were made on 100 random locations in SEM image using image analysis software ImageJ (National Institutes of Health, USA).

#### 2.3.5. Textural characterization

$N_2$ adsorption and desorption isotherms were obtained at 77 K on a Quantachrome Autosorb 1 sorption analyzer. All samples were outgassed for 16 h at 200 °C under high vacuum in the degas port of the adsorption analyzer. The specific surface area of the prepared samples was calculated from the $N_2$ adsorption isotherms using the multipoint Brunauer–Emmett–Teller (BET) technique. Textural pore size distribution and the mean pore diameter were derived using the Barrett–Joyner–Halenda (BJH) method. Total pore volumes were estimated from the adsorbed amount of $N_2$ at relative pressure of 0.995.

#### 2.3.6. Antibacterial tests

Antibacterial properties of all samples were investigated using the quantitative viable count method. The stock solution was prepared by mixing 1 mL *E. coli* with 9 mL of LB (Luria-Bertani) broth and incubated at 37 °C for 24 h with shaking at 250 rpm. 0.1 g BG powder was autoclaved and mixed with the stock solution. 0.1 mL of the prepared mixture was then inoculated on LB agar plates followed by incubation at 37 °C for 24 h. Finally, the number of colony-forming units were counted. The tests were carried out in triplicate. Student's *t*-test was used to evaluate the statistical significance amongst the data.

*2.3.7. Simulated body fluid test*

The *in vitro* bioactivity of samples was evaluated by immersing them in SBF solution prepared according to the method reported by Kokubo et al. [20]. The samples were immersed in SBF solution for 3,7 and 14 days.

The Scanning Electron Microscope (SEM, Hitachi, TM3000) at an operating voltage of 15 kV and EDX were used to study the morphology and the Ca/P ratio of the apatite formed on the surface of BG samples respectively.

## 3. Results and discussion

Two different types of BG were synthesized: pure BG (50Si), and BG containing varying amount of ceria (1Ce, 5Ce and 10Ce). Pure BG 50Si appeared white in color whereas light-yellow/cream color was observed for Ce containing samples. Their color intensities varied proportionally with the doping concentrations. Agglomeration of spherical particles having a mean diameter of 84 nm was observed for 50Si, while the mean diameter of spherical particles of 5Ce was 80 nm (Fig. 1). Fig. 2 shows the elemental composition obtained from EDX analysis of pure and Ce doped BG, the intensity of peak due to Ce increased with the increased doping concentration, confirming higher degree of metal substitution in the prepared BG as intended.

Generally, BG with heat treatment around 700 °C is expected to be amorphous as the crystallization is known to occur at temperature around 800 °C and above [21]. However, the XRD analysis of 50Si showed only one weak peak at $2\theta = 32^{\circ}$ which was assigned to calcium silicate, $Ca_2SiO_4$ (JCPDS # 29–0369) formed due to the partial crystallization during the calcinations process at 700 °C (Fig. 3) [22]. XRD patterns of 5Ce and 10Ce contained four major peaks assigned to the (1 1 1), (2 0 0), (2 2 0), (3 1 1) planes of ceria ($CeO_2$) [23], these peaks became more intense as the ceria concentration increased inside the BG (Fig. 3). On the other hand, 1Ce showed no diffraction peaks for ceria, this absence of diffraction pattern was attributed to the low amount of ceria present, which was below the detection range of the XRD instrument.

In the UV–vis spectra, it was observed that the band edge of the glass shifted towards the longer wavelength when cerium content was increased, from 1Ce to 10Ce, with band edge of 10Ce penetrating slightly into the visible region (Fig. 4). This absorption extension with cutoff wavelength around 450 nm was believed to be caused by the existence of ceria in +4 oxidation state [24,25]. This trend indicates that the preferred

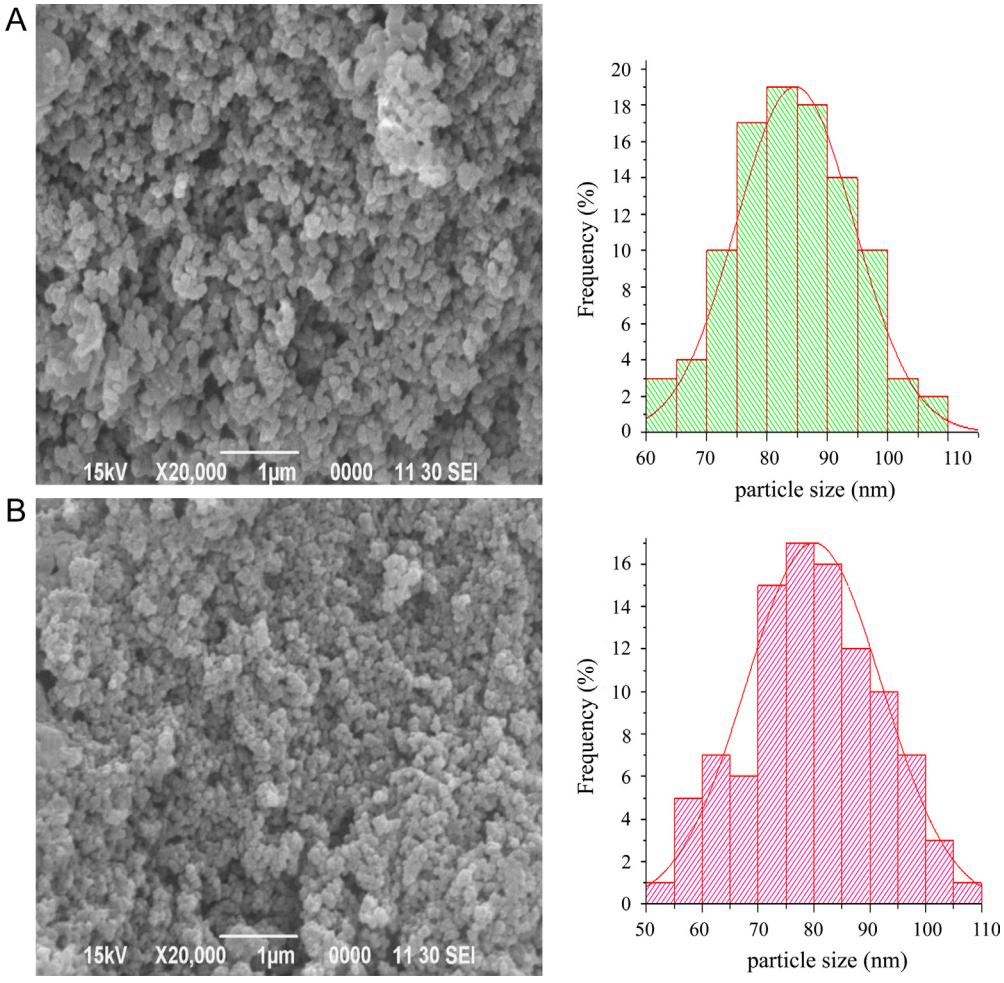


Fig. 1. SEM images of (A) 50Si (B) 5Ce and their particle size distribution.

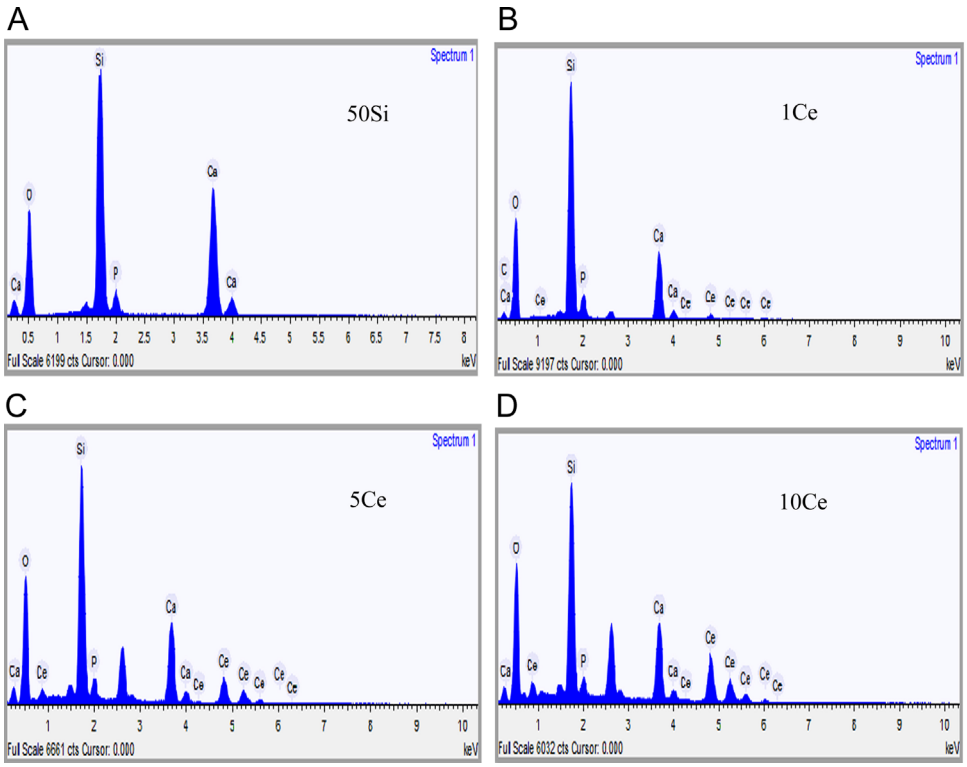


Fig. 2. EDX analysis of (A) 50Si (B) 1Ce; (C) 5Ce; and (D) 10Ce.

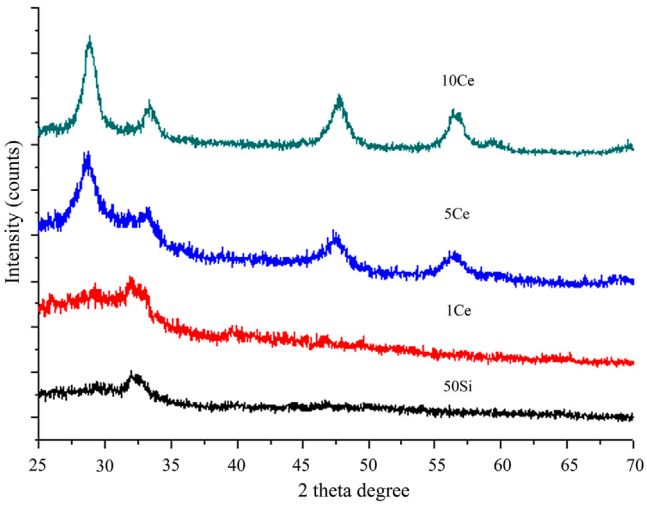


Fig. 3. XRD of (i) 50Si; (ii) 1Ce; (iii) 5Ce; and (iv) 10Ce.

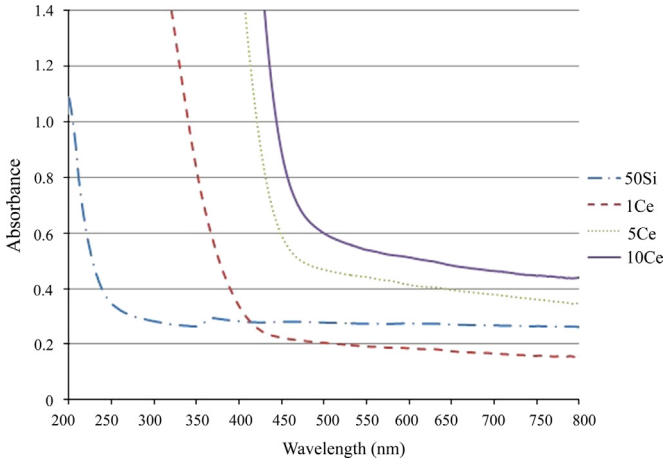


Fig. 4. UV–vis spectra.

oxidation of Ce changes from +3 to +4 as the Ce content inside the BG is increased. This trend observed in UV study is in accordance with XRD results discussed above which showed that Ce existed as $CeO_2$ in 10Ce.

FTIR spectra of all BG samples contained characteristic peaks attributed to Si–O–Si (Fig. 5). The broad vibration bands between 994–1075 $cm^{-1}$ and 500–520 $cm^{-1}$ were due to Si–O–Si asymmetric stretching and Si–O–Si bending respectively. The band at 921 $cm^{-1}$ is thought to be due to either Si–O–Ca or non-bridging oxygen (NBO) [26]. This band is not obvious in all samples due to an overlap with broad Si–O–Si peak. The peak observed near 600 $cm^{-1}$ was assigned to O–P–O bending of the phosphate group. The presence of phosphorus in the form of orthophosphate, $PO_4^{3-}$, was confirmed by the presence of absorption band at 570–600 $cm^{-1}$ which was attributed to $PO_4^{3-}$ antisymmetric bending. Furthermore, the incipient doublets at this region indicated that the orthophosphate are present in a crystal-like environment [26]. It is believed that the orthophosphate groups in isolated crystalline nano-regions weaken connectivity of glass structure and serve as nucleation sites in SBF [26]. Hygroscopic nature of silicate glasses was demonstrated through the presence of O–H symmetric stretching and bending vibration modes due to water were observed at around 3400 $cm^{-1}$ and 1630 $cm^{-1}$ respectively. Moderate absorption band was observed at

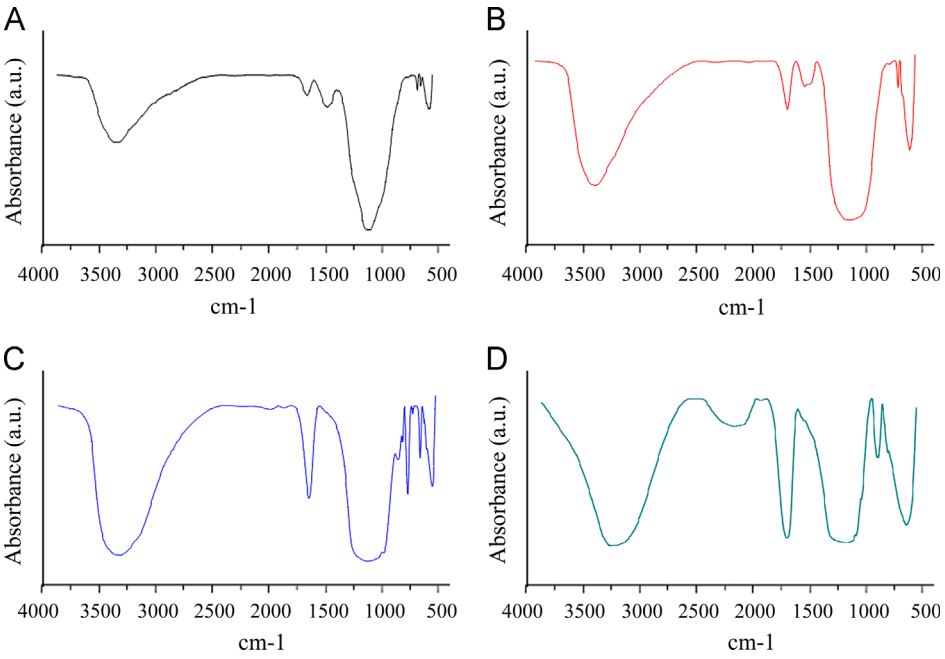


Fig. 5. FTIR of (A) 50Si, (B) 1Ce, (C) 5Ce, and (D) 10Ce.

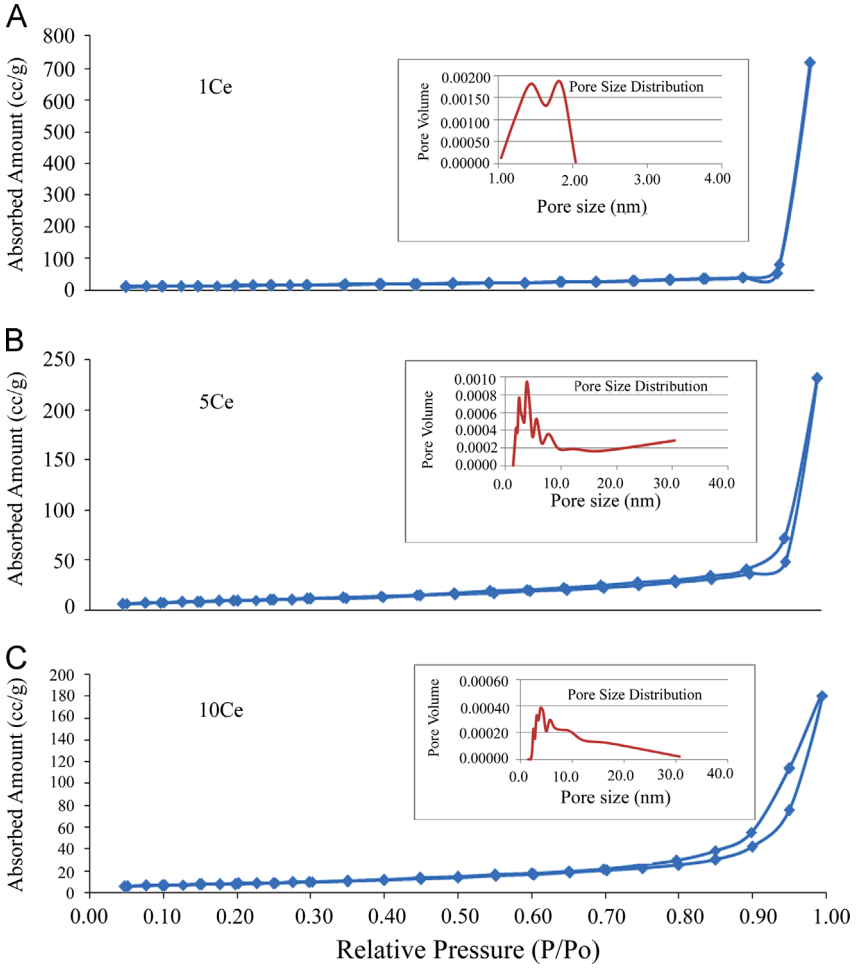


Fig. 6. $N_2$ adsorption–desorption isotherm.

803 $cm^{-1}$ for 5Ce and 10Ce which was not seen for other samples. This band was assigned to the O–Si–O bending mode of $SiO_4^{4-}$ [27]. Furthermore, the peak at 921 $cm^{-1}$ due to Si–O–M (M = metal ions) or NBO was only observed for 5Ce and 10Ce samples, indicating that the higher Ce content has disrupted the silicate network. The presence of orthosilicate species, $SiO_4^{4-}$ and NBO are known to promote glass leaching which is considered beneficial in promoting apatite formation, thus enhancing bioactivity [28].

Textures of samples were determined by analysis of nitrogen adsorption and desorption isotherms. The nitrogen adsorption–desorption isotherms of the samples are depicted in Fig. 6. According to IUPAC classification, isotherms for 5Ce and 10Ce are of type IV, indicating that the samples are mesoporous. Their curves are identifiable as type H1 hysteresis loops which is typical of a one-dimensional channel. The BET surface area, pore volume and average pore diameter were calculated from nitrogen adsorption and are listed in Table 2. The specific surface area decreased from 49.68 to 36.96 to 31.84 $m^2/g$ with increasing ceria content from 1% to 10%. This observation is supported by measurements of pore volume. The pore volume decreased accordingly from 1.109 to 0.360 to 0.280 $ccg^{-1}$. The reduction in the specific surface area and pore volume signifies that the framework of the mesoporous silica was disturbed by the incorporation of ceria. In addition, the average pore diameter first increased and then decreased. It can be seen from the pore size distribution curve of samples that the pore size of 1Ce was in microporous range while that of 5Ce and 10Ce a concentrated distribution between 3 and 4 nm was observed, which indicated that their pore sizes were in mesoporous range (Fig. 6). It is well known that the width of hysteresis loop is proportional to the pores interconnectivity. From Fig. 6, it can be seen that increasing ceria content resulted in wider hysteresis loops i.e. the incorporation of ceria has resulted in increased interconnectivity of the pores.

Table 2
Textural parameters obtained by $N_2$ adsorption measurement.

| Sample code | $S_{BET}$ ($m^2\ g^{-1}$) surface area | Pore volume ($ccg^{-1}$) | Avg. pore diameter (nm) |
|---|---|---|---|
| 1Ce | 49.68 | 1.109 | 1.667 |
| 5Ce | 36.96 | 0.360 | 3.813 |
| 10Ce | 31.84 | 0.280 | 3.075 |

Antibacterial property of all BG samples was investigated using quantitative viable count method. All samples at concentration 10 mg/mL were incubated with *E. coli* suspension for 24 h (Fig. 7). Previous studies have shown that high concentration of (100 mg/mL) of BG possessed antibacterial effect towards many types of bacteria [29–31]. This antibacterial effect of BG is attributed to the increase of pH level which reduces the viability of bacterial suspension [29]. However, in this study 50Si showed no antibacterial effect towards *E. coli* which was attributed to the very low concentration (10 mg/mL) of BG used in this study. However, 5Ce and 10Ce samples showed significant antibacterial effect ($p < 0.05$ for 5Ce and 10Ce as compared to 50Si). Increase in Ce content from 5 mol% to 10 mol% did not significantly enhance the antibacterial property. Although Garner et al. [10] concluded that cerium possess limited antibacterial properties, some although not many studies have provided strong evidence that cerium has microbicidal effects towards a panel of bacteria [32,33]. Cerium (III) ion has been reported to bind rapidly to *E. coli* cells, inhibit endogenous respiration of cells as well as penetrate into the cytoplasm of the cells and interfere with their metabolic functions. It is speculated that the interference of metabolic activity in the cell is due to the rapid combination of this rare earth metal ions with phosphate and protein compounds [34]. The penetration of $Ce^{3+}$ into the cells was confirmed by a study by Chen et al. which showed that permeability of outer and inner membrane was significantly increased by $Ce^{3+}$ [35]. It should be noted that the enhanced antibacterial properties shown in this study may be attributed to the coexistence of $Ce^{3+}$ and $Ce^{4+}$ in our samples. Previous research showed that adsorption of ceria particle takes place at the surface of *E. coli* cells followed by reduction of cerium (IV) to cerium (III), suggesting that oxidative stress

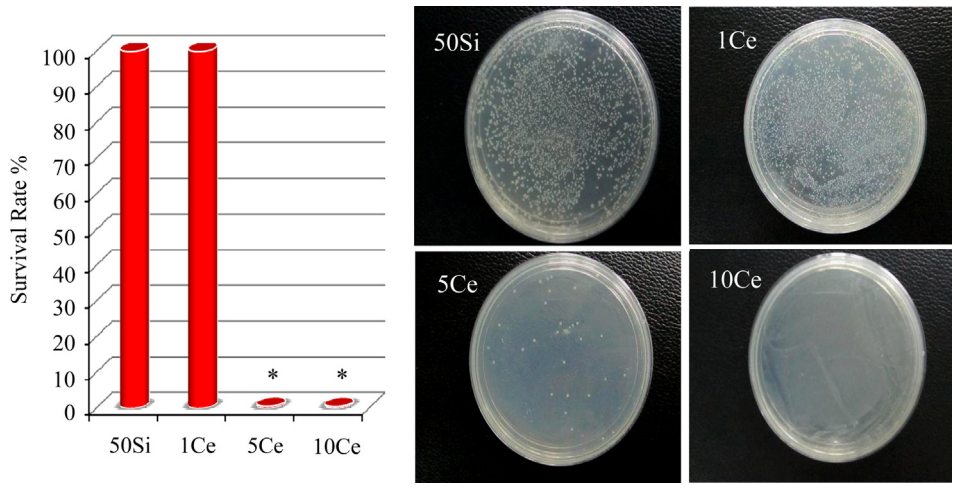


Fig. 7. Survival rate and Agar plates after incubation for 24 h; *$p < 0.05$ as compared to 50Si.

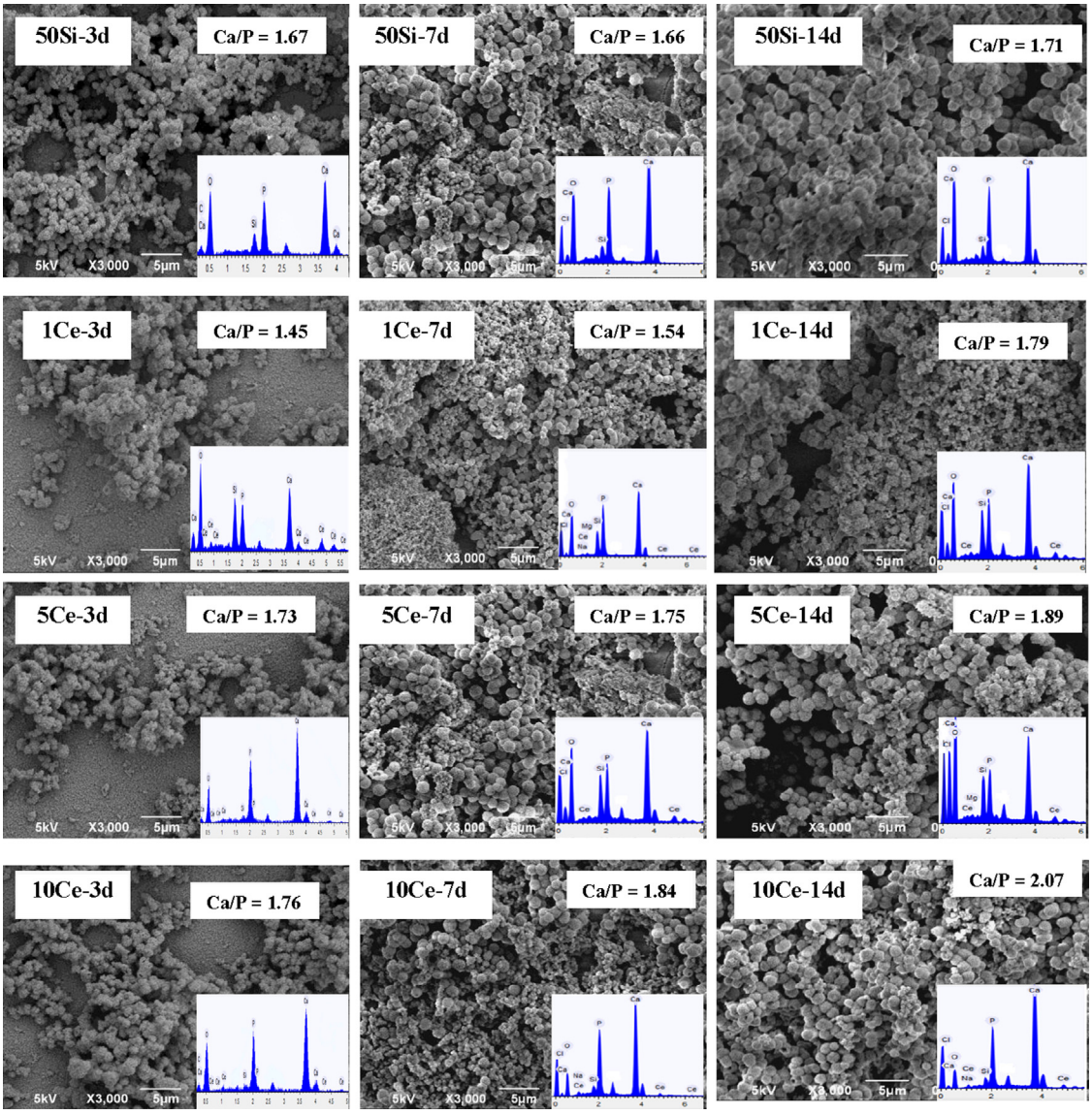


Fig. 8. SEM and EDX analysis of apatite formation upon immersion in SBF for 3, 7 and 14 days.

is the possible mechanism how ceria particle exerts its toxicity [36]. Attachment of ceria particle at the surface of cells could block the transport of essential nutrients leading to cell death [14] and might induce mechanical damage to the cell membrane [15]. In short, the direct contact of ceria particle and bacterial cells is the crucial factor to explain the toxicity of ceria towards *E. coli* [36,37]. The Ce doped BG synthesized in this study is considered to possess better antibacterial properties because it can act through 2 distinct mechanisms: ionic and particle effects. This is particularly important because in case one of the mechanisms was impeded due to environmental factor, e.g. particle effects diminished upon interaction or agglomeration with other particles in the medium [36,37], ionic effect could help to retain the antibacterial function of the material.

A widely used method for assessing the tendency of a material to bond to living human hard tissue is to assess the ability of the material to invoke the formation of bone-like apatite upon immersion in SBF. The bone-like apatite layer enables the materials to make direct contact with human bone living cells [38]. Fig. 8 shows the SEM and EDX analysis of the surface of the BG samples after immersion in SBF for 3, 7 and 14 days. The whole surface of all samples was covered

Table 3
Ca/P atomic ratio of apatite layer formed on the surface after immersion in SBF solution.

| Composition | Days | | |
|---|---|---|---|
| | 3 | 7 | 14 |
| 50Si | 1.67 | 1.66 | 1.71 |
| 1Ce | 1.45 | 1.54 | 1.79 |
| 5Ce | 1.73 | 1.75 | 1.89 |
| 10Ce | 1.76 | 1.84 | 2.07 |

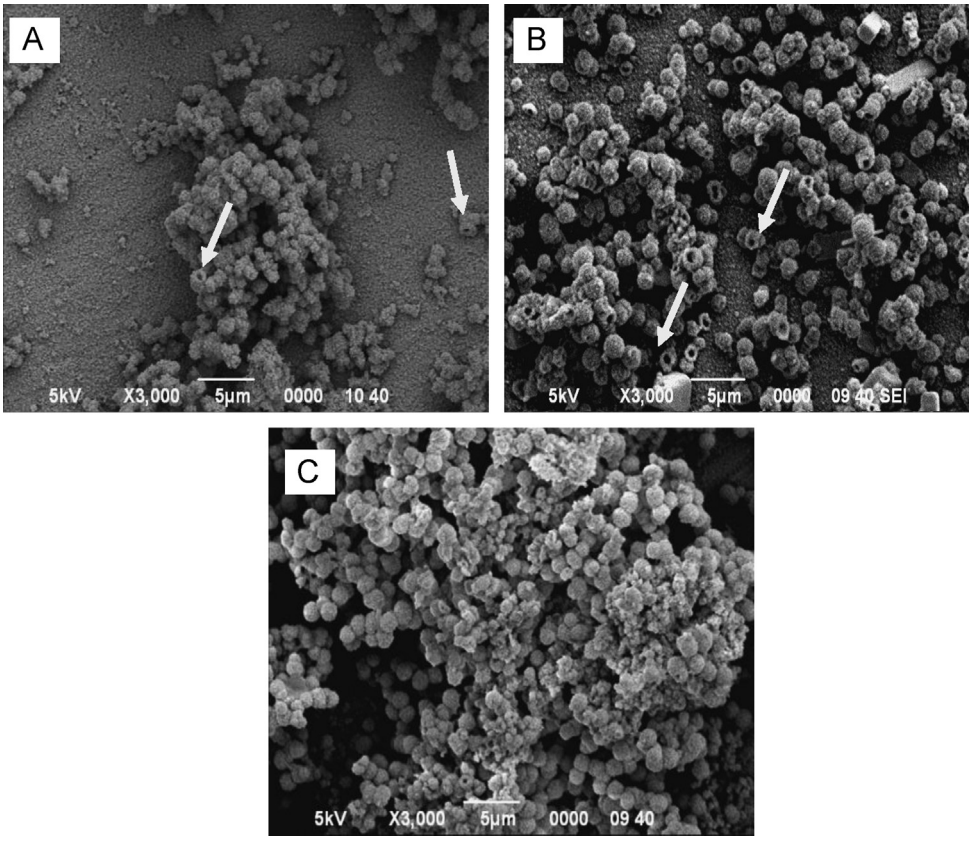


Fig. 9. SEM analysis of hollow apatite formation on 5Ce samples in SBF for (A) 3, (B) 7 and (C) 14 days at 3000× magnification.

with spherical apatite particles. EDX analysis showed that the newly formed layer predominantly consisted of calcium and phosphorus. Presence of silicon was also detected on the surface, which could be due to the formation of amorphous silica gel during the apatite formation process. Mechanism of apatite formation involves several steps: (i) exchange of calcium ions from surface with protons; (ii) silanol formation produced on surface; (iii) polymerization of silanol groups to produce amorphous silica gel; (iv) migration of calcium ions and phosphate ions to surface to form apatite, and (v) crystallization of apatite. EDX analysis of the surface after immersion in SBF for 3, 7 and 14 days showed that Ca/P ratio increased from 1.67 to 1.71 for 50Si, from 1.45 to 1.79 for 1Ce, whereas Ca/P ratio for 5Ce and 10Ce increased from 1.73 to 1.89 and from 1.76 to 2.07 respectively (Table 3, Fig. 8). The Ca/P values for 50Si and 1Ce samples are very close to the stoichiometric ratio of hydroxyapatite (1.67) after 14 days of SBF immersion. This indicates that the low content of ceria favors the formation of stoichiometric hydroxyapatite. Increasing the cerium content in BG resulted in the formation of calcium rich apatite layer over 14 days, this could be due to the release of cerium ion which in turn compete with Ca ions for the formation of respective phosphates [22]. Interestingly, it was found that the apatite layer formed on all samples consisted of hollow apatite spheres. Fig. 9 shows the representative growth process of the apatite particles from 3 to 14 days. It can be clearly observed that on day 3 and day 7, some apatite particles existed as hollow hemispheres (pointed out by white arrow), (Fig. 9A and B). The number of hemisphere present on the surface decreased as the immersion time increased to 14 days, when most of the apatite particles had grown into full spheres Fig. 9(C). To best of our knowledge, this is the first report of growth of hollow spherical apatite particles in SBF solution.

In conclusion, all samples containing ceria induced the formation of apatite layer with Ca/P ratio close to the stoichiometric HA [39], in addition 5Ce and 10Ce sample showed remarkable antibacterial activity against *E. coli* indicating that they are excellent candidates for application in the field of bone-regeneration.

## 4. Conclusion

BG containing ceria was successfully synthesized using cerium (III) chloride in this study. Cerium in BG can exist in $Ce^{3+}$ and $Ce^{4+}$ oxidation states, which depended on the initial cerium content in BG. Incorporation of cerium of above 5 mol% was able to impart BG with antibacterial properties. Antibacterial test using quantitative viable count method showed that 5Ce and 10Ce samples prevent bacterial colonization effectively after 24 h. Furthermore, the incorporation of ceria into BG has shown to result in good *in vitro* bioactivity, indicating the potential use of such biomaterial in bone regeneration field.

## Acknowledgments

Authors acknowledge the financial support from MyPhD scholarship (880330235485) from Ministry of Higher Education, Malaysia.

## References

[1] Z. Hong, A. Liu, L. Chen, X. Chen, X. Jing, Preparation of bioactive glass ceramic nanoparticles by combination of sol–gel and coprecipitation method, Journal of Non-Crystalline Solids 355 (2009) 368–372.
[2] P. Saravanapavan, J.R. Jones, R.S. Pryce, L.L. Hench, Bioactivity of gel–glass powders in the $CaO–SiO_2$ system: A comparison with ternary ($CaO–P_2O_5–SiO_2$) and quaternary glasses ($SiO_2–CaO–P_2O_5–Na$ 2O), Journal of Biomedical Materials Research Part B 66 (2003) 110–119.
[3] L.L. Hench, R.J. Splinter, W.C. Allen, T.K. Greenlee, Journal of Biomedical Materials Research Part A 5 (1971) 117.
[4] C. Ohtsuki, T. Kokubo, T. Yamamuro, Mechanism of apatite formation on $CaO–SiO_2–P_2O_5$ glasses in a simulated body fluid, Journal of Non-Crystalline Solids 143 (1992) 84–92.
[5] S. Srinivasan, R. Jayasree, K.P. Chennazhi, S.V. Nair, R. Jayakumar, Biocompatible alginate/nano bioactive glass ceramic composite scaffolds for periodontal tissue regeneration, Carbohydrate Polymers 87 (2012) 274–283.
[6] M. Mazrooei Sebdani, M.H. Fathi, Novel hydroxyapatite-forsterite-bioglass nanocomposite coatings with improved mechanical properties, Journal of Alloys and Compounds 509 (2011) 2273–2276.
[7] Q.Z. Chen, I.D. Thompson, A.R. Boccaccini, 45S5 Bioglass®-derived glass–ceramic scaffolds for bone tissue engineering, Biomaterials 27 (2006) 2414–2425.
[8] A.D. Pye, D.E.A. Lockhart, M.P. Dawson, C.A. Murray, A.J. Smith, A review of dental implants and infection, Journal of Hospital Infection 72 (2009) 104–110.
[9] A. Hoppe, N.S. Güldal, A.R. Boccaccini, A review of the biological response to ionic dissolution products from bioactive glasses and glass–ceramics, Biomaterials 32 (2011) 2757–2774.
[10] J.P. Garner, P.S.J. Heppell, Cerium nitrate in the management of burns, Burns 31 (2005) 539–547.
[11] Y. Lin, Z. Yang, J. Cheng, Preparation, characterization and antibacterial property of cerium substituted hydroxyapatite nanoparticles, Journal of Rare Earths 25 (2007) 452–456.
[12] X. Cai, G.-J. Dai, S.-Z. Tan, Y. Ouyang, Y.-S. Ouyang, Q.-S. Shi, Synergistic antibacterial zinc ions and cerium ions loaded α-zirconium phosphate, Materials Letters 67 (2012) 199–201.
[13] A. Chen, Q. Shi, J. Feng, Y. Ouyang, Y. Chen, S. Tan, Dissociation of outer membrane for Escherichia coli cell caused by cerium nitrate, Journal of Rare Earths 28 (2010) 312–315.
[14] O. Zeyons, A. Thill, F. Chauvat, N. Menguy, C. Cassier-Chauvat, C. Oréar, J. Daraspe, M. Auffan, J. Rose, O. Spalla, Direct and indirect $CeO_2$ nanoparticles toxicity for *Escherichia coli* and Synechocystis, Nanotoxicology 3 (2009) 284–295.
[15] N.J. Rogers, N.M. Franklin, S.C. Apte, G.E. Batley, B.M. Angel, J.R. Lead, M. Baalousha, Physico-chemical behaviour and algal toxicity of nanoparticulate $CeO_2$ in freshwater, Environmental Chemistry 7 (2010) 50–60.
[16] C. Leonelli, G. Lusvardi, G. Malavasi, L. Menabue, M. Tonelli, Synthesis and characterization of cerium-doped glasses and in vitro evaluation of bioactivity, Journal of Non-Crystalline Solids 316 (2003) 198–216.
[17] S. Shruti, A.J. Salinas, G. Malavasi, G. Lusvardi, L. Menabue, C. Ferrara, P. Mustarelli, M. Vallet-Regi, Structural and in vitro study of cerium, gallium and zinc containing sol–gel bioactive glasses, Journal of Materials Chemistry 22 (2012) 13698–13706.
[18] W. Xia, J. Chang, Preparation and characterization of nano-bioactive-glasses (NBG) by a quick alkali-mediated sol–gel method, Materials Letters 61 (2007) 3251–3253.
[19] A.M. El-Kady, A.F. Ali, Fabrication and characterization of ZnO modified bioactive glass nanoparticles, Ceramics International 38 (2012) 1195–1204.
[20] T. Kokubo, H. Kushitani, S. Sakka, T. Kitsugi, T. Yamamuro, Solutions able to reproduce in vivo surface-structure changes in bioactive glass–ceramic A-W3, Journal of Biomedical Materials Research Part A 24 (1990) 721–734.
[21] R.L. Du, J. Chang, S.Y. Ni, W.Y. Zhai, J.Y. Wang, Characterization and *in vitro* bioactivity of zinc-containing bioactive glass and glass–ceramics, Journal of Biomaterials Applications 20 (2006) 341–360.
[22] Y.F. Goh, A.Z. Alshemary, M. Akram, M.R. Abdul Kadir, R. Hussain, *In vitro* study of nano-sized zinc doped bioactive glass, Materials Chemistry and Physics 137 (2013) 1031–1038.
[23] S. Samiee, E.K. Goharshadi, Effects of different precursors on size and optical properties of ceria nanoparticles prepared by microwave-assisted method, Materials Research Bulletin 47 (2012) 1089–1095.
[24] C. Tang, Y. Bando, D. Golberg, R. Ma, Cerium phosphate nanotubes: synthesis, valence state, and optical properties, Angewandte Chemie International Edition 44 (2005) 576–579.
[25] A.S. Karakoti, O. Tsigkou, S. Yue, P.D. Lee, M.M. Stevens, J.R. Jones, S. Seal, Rare earth oxides as nanoadditives in 3-D nanocomposite scaffolds for bone regeneration, Journal of Materials Chemistry 20 (2010) 8912–8919.
[26] H. Aguiar, E.L. Solla, J. Serra, P. González, B. León, N. Almeida, S. Cachinho, E.J.C. Davim, R. Correia, J.M. Oliveira, M.H.V. Fernandes, Orthophosphate nanostructures in $SiO_2–P_2O_5–CaO–Na_2O–MgO$ bioactive glasses, Journal of Non-Crystalline Solids 354 (2008) 4075–4080.
[27] E. Zhang, C. Zou, G. Yu, Surface microstructure and cell biocompatibility of silicon-substituted hydroxyapatite coating on titanium substrate prepared by a biomimetic process, Materials Science and Engineering C 29 (2009) 298–305.
[28] J.M. Oliveira, R.N. Correia, M.H. Fernandes, Effects of Si speciation on the in vitro bioactivity of glasses, Biomaterials 23 (2002) 371–379.
[29] I. Allan, H. Newman, M. Wilson, Antibacterial activity of particulate Bioglass® against supra- and subgingival bacteria, Biomaterials 22 (2001) 1683–1687.
[30] E. Munukka, O. Leppäranta, M. Korkeamäki, M. Vaahtio, T. Peltola, D. Zhang, L. Hupa, H. Ylänen, J. Salonen, M. Viljanen, E. Eerola, Bactericidal effects of bioactive glasses on clinically important aerobic bacteria, Journal of Materials Science: Materials in Medicine 19 (2008) 27–32.
[31] V. Mortazavi, M.M. Nahrkhalaji, M.H. Fathi, S.B. Mousavi, B.N. Esfahani, Antibacterial effects of sol–gel-derived bioactive glass nanoparticle on aerobic bacteria, Journal of Biomedical Materials Research Part A 94A (2010) 160–168.
[32] S. Burkes, C.S. Mccleskey, The bacteriostatic activity of Cerium, lanthanum, and thallium, Journal of Bacteriology 54 (1947) 417–424.
[33] L. Cobrado, A. Silva-Dias, M.M. Azevedo, C. Pina-Vaz, A.G. Rodrigues, In vivo antibiofilm effect of cerium, chitosan and hamamelitannin against usual agents of catheter-related bloodstream infections, Journal of Antimicrobial Chemotherapy., (2012).
[34] J.M. Sobek, D.E. Talburt, Effects of the rare earth cerium on *Escherichia coli*, Journal of Bacteriology 95 (1968) 47–51.
[35] A. Chen, Q. Shi, Y. Ouyang, Y. Chen, Effect of $Ce^{3+}$ on membrane permeability of *Escherichia coli* cell, Journal of Rare Earths 30 (2012) 947–951.
[36] A. Thill, O. Zeyons, O. Spalla, F. Chauvat, J. Rose, M. Auffan, A.M. Flank, Cytotoxicity of $CeO_2$ nanoparticles for *Escherichia coli*. Physico-chemical insight of the cytotoxicity mechanism, Environmental Science and Technology 40 (2006) 6151–6156.
[37] I. Rodea-Palomares, K. Boltes, F. Fernández-Piñas, F. Leganés, E. García-Calvo, J. Santiago, R. Rosal, Physicochemical characterization and ecotoxicological assessment of $CeO_2$ nanoparticles using two aquatic microorganisms, Toxicological Sciences 119 (2011) 135–145.
[38] C. Ohtsuki, H. Kushitani, T. Kokubo, S. Kotani, T. Yamamuro, Apatite formation on the surface of ceravital-type glass-ceramic in the body, Journal of Biomedical Materials Research Part A 25 (1991) 1363–1370.
[39] R.K. Singh, A. Srinivasan, Apatite-forming ability and magnetic properties of glass-ceramics containing zinc ferrite and calcium sodium phosphate phases, Materials Science and Engineering C 30 (2010) 1100–1106.